Quantum Electronics **41** (9) 769–775 (2011)

LASERS

PACS numbers: 42.55.Px; 42.60.Da; 42.60.Jf; 85.35.Be
DOI: 10.1070/QE2011v041n09ABEH014624

Modelling of a diode laser with a resonant grating of quantum wells and an external mirror

D.V. Vysotskii, N.N. Elkin, A.P. Napartovich, V.I. Kozlovskii, B.M. Lavrushin

Abstract. **A three-dimensional numerical model of a diode laser with a resonant grating of quantum wells (QWs) and an external mirror is developed and used to calculate diode laser pulses that are long compared to the time of reaching a stationary regime and are short enough to neglect heating of the medium. The consistent solutions of the Helmholtz field equation and the system of diffusion equations for inversion in each QW are found. A source of charge carriers can be both an electron beam and a pump laser beam. The calculations yielded the longitudinal and radial profiles of the generated field, as well as its wavelength and power. The effective threshold pump current is determined. In the created iteration algorithm, the calculation time linearly increases with the number of QWs, which allows one to find the characteristics of lasers with a large number of QWs. The output powers and beam divergence angles of a cylindrical laser are calculated for different cavity lengths and pump spot radii. After calculating the fundamental mode characteristics, high-order modes were additionally calculated on the background of the frozen carrier distributions in the QW grating. It is shown that all the competing modes remain below the excitation threshold for the pump powers used in the experiment. The calculated and experimental data for the case of pumping by a nanosecond electron beam are qualitatively compared.**

Keywords: *resonant heterostructure, method of counterpropagating waves, eigenvalues, nonlinear operator.*

1. Introduction

Heterostructures with a large number of quantum wells (QWs) are of practical interest for application in vertical-cavity surface-emitting lasers (VCSELs) with an external mirror. They can be pumped by either electron beams or laser diodes [1]. Both types of pumping can be identically simulated by introducing an effective pump current [2]. Longitudinally electron-beam-pumped diode lasers can be used in display technologies as quasi-cw monochromatic light sources [3, 4]. A distinguishing feature of these lasers is the absence of optical confinement in the direction perpendicular to the cavity axis. The transverse laser filed distribution is determined by the variation of the complex permittivity [5], which, in turn, is controlled by the distribution of the effective pump current density. The external mirror stabilises the spatial field distribution of the generated mode. Modelling of a VCSEL with a QW grating and an external mirror is a complicated computational problem due to the complex geometry of the laser structure and a nonlinear character of equations in partial derivatives with eigenvalues. A VCSEL structure contains a large number of layers, whose interfaces partially reflect light. In the active-medium layers, the electromagnetic field equations must be solved self-consistently with nonlinear diffusion equations for current carriers. A mathematical model of the laser must adequately take into account all the above circumstances.

The authors of [6] described a method of calculating a VCSEL with two Bragg mirrors and a small number of QWs, which was based on the use of counterpropagating waves and on the circumstance that the propagation of plane waves through a set of homogeneous quarter-wave layers of the Bragg mirror can be easily calculated using the transfer-matrix (T-matrix) formalism. The amplitudes of counterpropagating waves at the lower and upper interfaces of the set of layers are related to each other by a matrix that is a product of T-matrices with dimensions 2×2. One can expand the spatially inhomogeneous fields into plane waves and apply the T-matrix to the expansion components. Starting from some plane and making one round trip of the cavity using this transform, one can close the system of equations. In the obtained system of equations, the sought function is the field distribution of the wave of one direction in a chosen reference plane. In the discrete approximation, the authors of [6] reduced the problem to solving the matrix equation $A\boldsymbol{u} = 0$ for a finite-dimensional vector $\boldsymbol{u}$ that describes the field in a reference plane. The explicit expressions derived for the elements of the highly dimensional matrix A contained an unknown parameter, namely, an eigenvalue λ that determines the exact value of the optical mode frequency. The matrix equation $A\boldsymbol{u} = 0$ can be solved by fitting λ. This method requires a large memory for calculating the completely filled matrix A and, in addition, it is useless for describing optically nonlinear media, which are of most interest for modelling of lasers.

An ideologically similar method of calculating active VCSEL structures with a small number of QWs, which is free of the above drawbacks, was described in [7, 8]. It is well known that conventional two-mirror optical cavities without dispersive elements can be efficiently calculated by the Fox–Li iteration method [9], which also allows one to take into account nonlinear interaction with medium. The trans-

D.V. Vysotskii, N.N. Elkin, A.P. Napartovich State Research Center of Russian Federation 'Troitsk Institute for Innovation and Fusion Research', ul. Pushkovykh 12, 142190 Troitsk, Moscow region, Russia; dima@triniti.ru, elkin@triniti.ru, napart@mail.ru;
V.I. Kozlovskii, B.M. Lavrushin P.N. Lebedev Physics Institute, Russian Academy of Sciences, Leninsky prosp. 53, 119991 Moscow, Russia; e-mail: vikoz@sci.lebedev.ru, blavr@sci.lebedev.ru

Received 1 April 2011
Kvantovaya Elektronika **41** (9) 769–775 (2011)
Translated by M.N. Basieva

formation of a filed passing from one transverse plane to another in a layered medium is described by simple reflection conditions at interfaces. A change in the field passing through a QW with an inhomogeneous charge distribution determined from the solution of the diffusion equation is described by a nonlinear operator, because of which the problem must be solved by iterations. For a heterostructure consisting of multiple QWs, the problem is more complicated. To solve this problem, we developed a special iteration procedure in which the time needed for solving the problem linearly depends on the number of QWs [10].

In the present work, the iteration algorithm [10] is generalised to the case of a VCSEL with a large number of QWs and an external mirror. The calculated profiles and frequency spectrum of the cavity modes for a cylindrical VCSEL are presented. The limits of stable single-mode lasing are determined. A qualitative comparison with experiment is performed.

2. Mathematical model of a VCSEL with an external mirror

The heterostructure of a VCSEL with an external mirror consists of a Bragg mirror and a grating of QWs separated by barrier layers, from which generated carries diffuse into QWs (Fig. 1). If the z axis is directed perpendicular to the substrate, we can represent the VCSEL as a pile of plane layers $\{[z_{k-1}, z_k]$, $k = 1, \ldots, \mathcal{L}$, where $\mathcal{L}$ is the total number of layers, $\{z_k, k=0, \ldots, \mathcal{L}\}$ is the sequence of coordinates of interfaces between the layers, and $h_z = z_k - z_{k-1}$ is the thickness of the kth layer. The number $k = 0$ is given to the infinitely thick aluminum layer of the structure. The refractive index and the absorption coefficient are assumed to be homogeneous in all the passive layers. The gain and refractive profiles depend on pumping and emission.

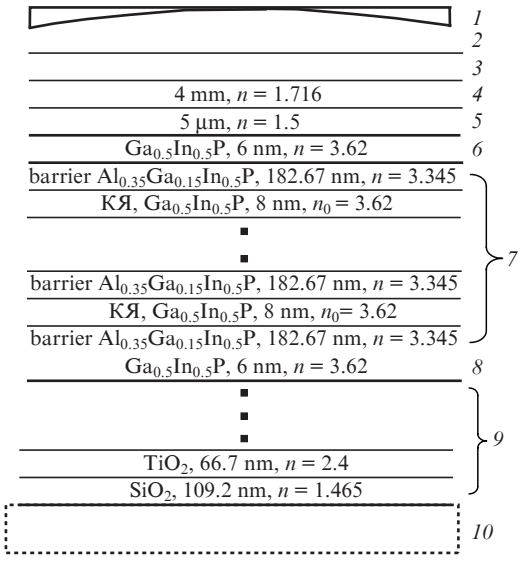

Figure 1. Schematic of a VCSEL with an external mirror (relative dimensions of layers are shown unscaled): (*1*) external mirror; (*2*) air gap; (*3*) antireflection coating; (*4*) sapphire disk; (*5*) glue layer; (*6*, *8*) protective layers; (*7*) heterostructure with a resonance grating of 25 QWs; (*9*) Bragg mirror consisting of 7.5 quarter-wave layer pairs; (*10*) aluminum substrate.

In this study, we neglect polarisation effects and restrict ourselves to the scalar diffraction model. It was also assumed that the laser structure has an axial symmetry, which makes it convenient to use cylindrical coordinates. The time dependence of the field at the frequency ω for a smooth field-amplitude envelope can be represented in the form $E(r,\varphi,z,t) = U(r,\varphi,z)\exp(-i t\Omega)$, $\Omega = \omega_0 + \Delta\omega - i\delta$, where ω_0 is the reference frequency, $\Delta\omega = \omega - \omega_0$ is the mode frequency shift, and δ is the decay decrement. The frequency ω_0 is chosen to be equal to the transition frequency. The corresponding reference values of the wave vector and wavelength in vacuum are determined conventionally, $\omega_0 = k_0 c$, $k_0 = 2\pi/\lambda_0$.

Taking into account the circular symmetry of pumping, the angular dependence of the field amplitude in the small-signal approximation can be represented in the form $U(r,\varphi,z) = U_m(r,z)\exp(im\varphi)$ (m is the angular harmonic number), and $U_m(r,z)$ satisfies the equation

$$\frac{\partial^2 U_m}{\partial z^2} + \frac{1}{r}\frac{\partial}{\partial r}\left(r\frac{\partial U_m}{\partial r}\right) - \frac{m^2}{r^2}U_m + (k_0^2 n^2 - ik_0 g)U_m - ik_0 n^2 \xi U_m = 0.$$

Here, $\xi = \mu + i2\Delta\kappa$ is the complex eigenvalue; $\Delta\kappa = \Delta\omega/c$; $\mu = 2\delta/c$ is the difference between the threshold and actual mode gains (hereinafter, mode decrement; $\mu > 0$ corresponds to the subthreshold regime); n and g are the refractive index and the gain with pump-induced components in the absence of saturation by the laser field.

To complete the statement of the problem, it is necessary to impose a boundary condition at the side boundary ($r = r_{\max}$) and at the output mirror. If $r_{\max}$ is so large that the influence of the side boundary on the solution is weak, then the field at the side boundary ($r = r_{\max}$) can be assumed to be zero.

Above-threshold pumping ($\mu < 0$) leads to lasing at the corresponding mode. The steady-state field of the axially symmetric fundamental mode also satisfies Eqn (1) at $m = 0$. However, the refractive index and the gain in each QW are not given values any more, but must be found from the following system of nonlinear diffusion equations for carriers in the pth QW [11]:

$$\frac{D}{r}\frac{\partial}{\partial r}\left(r\frac{\partial Y_p}{\partial r}\right) - \frac{Y_p}{\tau_{\rm nr}} - BN_{\rm tr}Y_p^2 - \frac{|U_{0,p}|^2 \ln(\chi(Y_p))}{\tau_{\rm nr}} = -\frac{j}{edN_{\rm tr}}, \quad p = 1, \ldots N_{\rm qw}.$$

Here, $Y_p = N_p/N_{\rm tr}$ is the normalised carrier density; N_p is the carrier density; $N_{\rm tr} = \left[-\tau_{\rm nr}^{-1} + \sqrt{\tau_{\rm nr}^{-2} + 4Bj_{\rm tr}/(ed)}\right]/(2B)$ is the transparency carrier density; $j_{\rm tr}$ is the effective transparency current density; D is the diffusion coefficient; $\tau_{\rm nr}$ is the nonradiative recombination time; B is the nonlinearity coefficient (for radiative recombination); e is the elementary electric charge; d is the QW thickness; $N_{\rm qw}$ is the total number of QWs; $j = Jf(r/r_0)/(2\pi)\int f(r/r_0)r\,dr$ is the equivalent density of the injection current creating the same flux of charge carriers in the QW as a pumping electron or laser beam of a given density; J is the total equivalent current, which, in these calculations, is taken to be identical in all QWs; $f(\rho)$ is the pump profile function; $f(0) = 1$; $\rho = r/r_0$; and r_0 is the effective radius of the pump region. The radiation intensity $I_{\rm p}$ in the pth QWs is assumed to be normalised to the saturation intensity $I_{\rm s} =$

$(hc/\lambda_0)[N_{tr}/(g_0\tau_{nr})]$, so that $|U_{0,p}|^2 = I_p/I_s$. At the side boundaries of the active layers ($r = r_{max}$), we impose zero boundary conditions for $Y_p(r)$. The refractive indices and the gains in active layers are calculated by the iteration formulas

$$g_p = g_0 \ln(\chi(Y_p)),$$

$$n_p = n_0 - \frac{R(g_p - g_{min})}{2k_0}, \qquad (3)$$

$$\chi(Y) = \begin{cases} \alpha + (1-\alpha)\, Y^{1/(1-\alpha)}, & Y < 1, \\ Y, & Y \geqslant 1, \end{cases}$$

where $\alpha = \exp(g_{min}/g_0)$; g_0 is a parameter with the gain dimensionality; g_{min} is a negative value corresponding to the absorption of laser radiation in a QW in the absence of pumping; n_0 is the QW refractive index in the absence of charge carriers; and R is the line broadening factor.

The equivalent injection current density is related to the electron-beam current density by the formula [7]

$$j = \frac{\varkappa j^b E_e}{3E_g N_{qw}},$$

where j^b is the axial electron-beam current density in A cm^{-2}, E_e is the beam-electron energy in eV, E_g is the energy gap width of barrier layers, and $\varkappa = 0.75$ is the portion of pump-electron energy transferred to the structure with QWs. The remaining energy is carried away by reflected and secondary-emission electrons and is absorbed in the Bragg mirror. For the experimental parameters $E_e = 40$ eV, $3E_g = 7.08$ eV, and $N_{qw} = 25$, the equivalent injection current density and the electron-beam current density are related by the expression

$$j = 170 \text{ A cm}^{-2} \longleftrightarrow j^b = 1 \text{ A cm}^{-2}.$$

Eqns (1)–(3) and the corresponding boundary conditions for $m = 0$ determine the eigenvalues and nonlinear operator functions. In the steady-state lasing regime, the condition $\mu = 0$ ($\mathrm{Re}\,\xi = 0$) must be fulfilled. The procedure of solving Eqn (1) with this condition is described in detail in [10], and here we present the general scheme of solving.

The total wave field in each horizontal plane within the limits of barriers and homogeneous structural layers is represented in the form of a sum of two waves propagating up and down the structure. Each of the waves is found by separating the components with positive and negative projections of the wave vector on the vertical axis in the three-dimensional Fourier image of the field. The field propagation between two neighbouring QWs is calculated using the T-matrix formalism for Fourier components, which ensures a fast calculation of the round-trip operator. The field propagation through QWs is calculated by transformation from Fourier to physical space at the QW boundaries using the fast Hankel transform algorithm [12] and by solving the one-dimensional Helmholtz equation with the boundary conditions at the QW boundaries that correspond to the local radial coordinate. This approach is justified when the QW thickness is considerably smaller than the field wavelength.

The use of an external mirror makes it necessary to include into the calculation the filed propagation to this mirror, the reflection by the spherical mirror, and the backward propagation to the structure. In the theory of two-mirror cavities [12–14], one usually uses the paraxial optics approximation in which the field propagation is described by a parabolic operator, which allows one to explicitly relate the distributions of fields in two separate planes. In this case, the possibility of taking into account the interference of counterpropagating waves, which plays a key role in resonant QW gratings, is lost. In our technique of calculating the filed propagation inside an active structure, we do not use the paraxial optics approximation, which eliminates the mentioned problem. To unify the calculation algorithm, we also solved the Helmholtz equation in the external part of the cavity and described the reflection from the output mirror by transferring the reflection boundary condition at the curved mirror to the reference plane transversely to the optical axis. The applicability of this approximation, which is widely used in the theory of two-mirror cavities [12, 13], was verified by us in test calculations. It was found that the accuracy of this approximation is acceptable for the entire region of the external cavity parameters. Thus, the described procedure allows us to determine the round-trip operator.

Our approach, which is based on the unified solution of the Helmholtz equation beyond the parabolic approximation, allows one to find the mode spectrum for composite cavities, including cavities almost randomly filled by plane layers with smoothly changing properties in the transverse plane.

The condition of field reproduction after a round trip is described by the operator equation

$$\boldsymbol{P}(g, n, \xi)u = u \qquad (4)$$

for the function u with the complex eigenvalue ξ. The positive or negative real part of ξ determines the field decay or growth rate, respectively. The imaginary part of ξ determines the frequency spectrum of optical modes. In addition to the wave field, the round-trip operator $\boldsymbol{P}$ includes the sought distributions of gains g and refractive indices n in the entire volume of the structure, as well as the eigenvalue ξ. The method of solving the obtained system of equations is described in [10] and, due to its complexity, is not given in this paper.

3. Experimental data

The active part of the VCSEL contained 25 QWs ($Ga_{0.5}In_{0.5}P$, 8 nm) separated by barrier layers ($Al_{0.35}Ga_{0.15}In_{0.5}P$, $h \approx 182.7$ nm) (Fig. 1). Thus, the QW grating represented a finite periodic structure with the optical period length equal exactly to $\lambda_0 = 640$ nm. From the top and bottom, the active part of the VCSEL was bounded by protecting GaInP layers with the thickness $h = 6$ nm, which protected the upper and lower barrier layers from oxidation in the process of the active element fabrication. In the experiment with electron-beam pumping, the lower protecting layer was adjacent to a Bragg mirror consisting of 7.5 pairs of alternating quarter-wave SiO_2/TiO_2 layers. The lower SiO_2 layer was coated by an Al layer 1 μm thick. The electron-beam pumping was performed through layers 8–10 (Fig. 1). The upper surface of the structure was glued to a (0001)-oriented sapphire disk 4 mm thick, which was the optical window of the laser. The glue layer had a thickness of 55 μm and a refractive index of 1.5. The outer surface of the sapphire disk was antireflection coated. The external spherical mirror had a diameter of 1.5 cm, a plane outer surface, and a concave inner surface with a curvature radius of 3 cm, which was used as a substrate for deposition

of the second semitransparent Bragg mirror consisting of SiO_2/TiO_2 quarter-wave layers. The number of layers was varied to achieve refection coefficients in the region of 0.95–0.99.

The laser operated in a pulsed regime due to insufficiently efficient heat removal and a relatively high lasing threshold. Due to a specific feature of the laser, the pulsed regime was achieved by periodic scanning of the electron-beam spot along a line segment 3 mm long. The excitation pulse duration for an individual point of the line was determined by the electron-beam diameter and the scanning rate (10^5 cm s^{-1}); the scanning frequency was 50 Hz. The line segment was moveable along the active element surface. A pulse falling into the region of a cavity mode excited a laser pulse, whose typical shape in the case of the electron-beam spot diameter of 40 μm is shown in Fig. 2. The laser pulse duration can be increased to 100 ns by using a larger electron-beam spot and a lower scanning rate. The total electron-beam current was changeable within a range of 0–2.5 mA at the electron energy from 30 to 50 keV. The electron-beam diameter was changed within a range of 25–100 μm by changing the focusing current in an electromagnetic focusing lens.

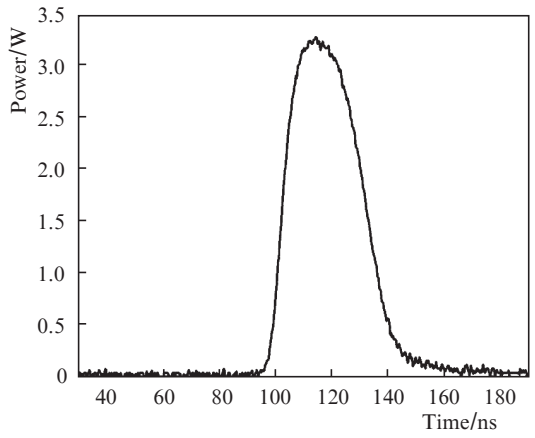

Figure 2. Laser pulse time profile at r_0 = 40 μm, L = 2.5 cm, and J^b= 2 mA.

A characteristic laser pulse spectrum is shown in Fig. 3. The main peak in the spectrum corresponds to a wavelength of 644.4 nm, and the width of the spectrum at the level of 10% is approximately equal to 1.3 nm. The structure of the spectrum is caused by the use of the external cavity and by an imperfect antireflection coating of the outer surface of the sapphire layer.

The laser beam structure in the far-field zone depended on the optical length of the cavity, on the diameter of the excitation region, and on the quality of alignment of the external mirror. In a well-aligned cavity with an optical length considerably smaller than the curvature radius of the external mirror, the far-field distribution usually had one peak with an angular divergence of 7.5 mrad, which is close to the diffraction limit.

The laser power reached 3.2 W at the output mirror reflectivity of 0.985. It also depended on the cavity length L and the radius of the excited region. When this radius was small ($r_0 \approx 15$ μm), a stable lasing was observed in the range of L = 2.8–3.0 cm (nearly semiconcentric cavity), when the size of the excitation region was comparable with the transverse size

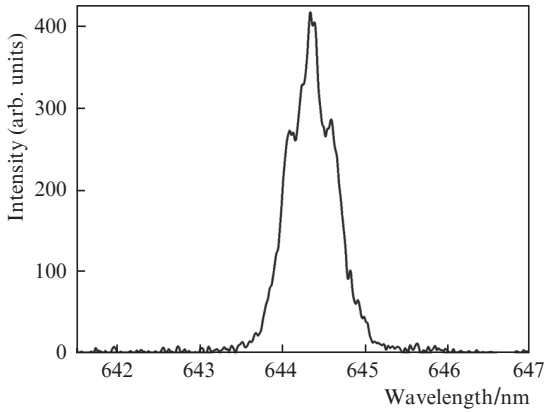

Figure 3. Experimental laser radiation spectrum at r_0 = 40 μm, L = 2.5 cm, and J^b = 2 mA.

of generated cavity modes. A significant excess of the transverse dimensions of the fundamental mode over the excitation region diameter (which occurred at L < 2.8 cm) lead to suppression of lasing. At the excitation region radius of 40 μm, we observed a weak dependence of the laser power on the cavity length in a wide range (L = 1.0–3.0 cm). We also measured the laser power at L = 2.0 cm with an electron-beam current J^b = 2 mA (equivalent current J = 340 mA) as a function of the electron-beam radius at the active laser element. In the case of strong focusing (small beam radius), lasing did not occur, despite the fact that the excitation density was maximal. Lasing began at a weaker focusing. The maximum power was achieved at $r_0 \approx 40$ μm. With further defocusing of the electron beam, the laser power decreased again due to a strong decrease in the excitation density.

4. Calculation results and discussion

Calculations were performed with the following values of parameters entering Eqns (1) and (2): D = 0.5 cm^2 s^{-1}, τ_{nr} = 1 ns, $B = 3.5\times10^{-10}$ cm^3 s^{-1}, R = 2.5, g_0 = 3400 cm^{-1}, g_{min} = −1000 cm^{-1}, and $j_{tr} = 400$ A cm^{-2}. At these parameters, the saturation intensity was $I_s = 172$ kW cm^{-2}. Since precise data on the pump profile function were unknown, the calculations were performed for a model profile $f(\rho) = (1+\rho^4)^{-1}$, which was assumed to be constant along the length of the structure. The effective transparency current density corresponds to the axial density of the electron-beam transparency current j^b_{tr} = 2.35 A cm^{-2}. In most calculations, the external mirror diameter is taken to be 0.4 mm, the amplitude reflectivity of the surface is 0.985, and the curvature radius is 3 m. An increase in the mirror diameter lead to a strong increase in the calculation time due to a smaller discrimination of high-order modes.

Optical modes of a VCSEL were denoted by standard symbols TEM_{nm}, where m is the angular index corresponding to the dependence $\sim\exp(im\varphi)$ and n is the radial number. The number of nodes of the radial digital network was N_r = 1024 for all presented calculation results.

4.1. Calculation of nonlinear laser characteristics

In the considered case, the mode spectrum is not separated into purely longitudinal and purely transverse modes. In other words, a change in the field carrier frequency changes both the longitudinal and transverse mode structures. Nevertheless, the longitudinal structure of the laser optical

modes, which is determined by the total contribution of the Bragg laser dispersion, the resonance QW structure, and the distance to the external mirror can be separated in the limit of large pump region radius. In this case, one can represent the field in the form of counterpropagating plane waves and calculate the small-signal round-trip gain as a function of the radiation wavelength. A result of such calculation is shown in Fig. 4 for a heterostructure in which QWs form homogeneous layers with constant gains (g_0 = 3400 cm^{-1}) and refractive indices (n_0 = 3.62). The linear gain spectrum G shown in Fig. 4 is determined as the ratio of the intensity of the wave reflected from the structure to the intensity of the plane wave incident from the side of the external mirror. The central peak corresponds to the resonance mode of the structure, for which the total intensity in each QW is twice as high as the average intensity in the structure, which leads to an increase in the effective gain. In addition, the effect of the constructive interference in QWs with a high refractive index leads to an increase in the effective refractive index and to a shift of the resonance wavelength by 2.3 nm from the reference point 640 nm. The other peaks, whose height is approximately twofold smaller that the level G = 1, lie approximately periodically with an interval of 14 nm. They appear due to a shift of interference fringes with respect to the QW grating with changing wavelength. The fall of the gain at the spectrum edges relates to the width of the reflection band of the Bragg mirror ($\sim$ 190 nm). Here, we did not take into account the material gain dispersion since lasing occurred at close-to-resonance wavelengths with a width noticeably smaller than the material gain linewidth (see Fig. 3).

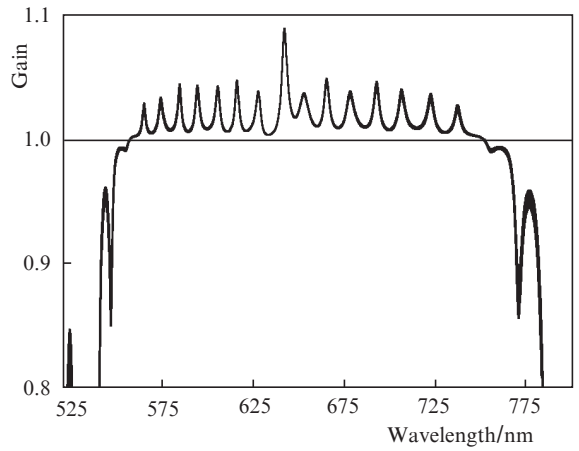

Figure 4. Dependence of the linear plane wave gain G on the incident radiation wavelength at L = 3 cm and a QW gain of 3400 cm^{-1}.

As was mentioned above, the radial inhomogeneity caused by the finiteness of the pump spot radius leads to a change in the longitudinal structure and to the appearance of a transverse structure of optical modes. Due to the nonlinearity of the lasing process, it is very difficult to separate the effect of individual variable parameters on the laser characteristics. To clarify the role of the amplitude and the gain profile, we calculated the linear amplification regime. In these calculations, we also found such important characteristics as the lasing threshold and the above-threshold mode discrimination as functions of the pump beam diameter and the distance to the mirror.

Let us illustrate the calculation results in the case with an equivalent pump current of 400 mA (the corresponding electron-beam current in the pulse peak is 2.35 mA). Figure 5 shows the TEM_{00} and TEM_{01} mode decrements for three pump beam radii versus the optical distance L from the upper surface of the heterostructure to the spherical mirror (in what follows, we call L the distance to the mirror). Since the medium is amplifying, the equality of the mode decrement to zero means that the mode has reached the lasing threshold, while a negative value means that the threshold is exceeded. Recall that the mode decrement in this paper is determined from the field decay rate in the laser. As follows from Fig. 5, the gain for the fundamental mode at a small pump spot radius (r_0 = 20 μm) exceeds the threshold value in the range L = 2.6–2.9 cm. As the mirror becomes closer to its position for a semiconcentric cavity (L = 3 cm), losses at the mirror edge increase. At distances smaller than 2.6 cm, the mode gain decreases due to broadening of the field distribution. As the pump spot diameter increases to 35 μm, the fundamental mode turns out to exceed the excitation threshold for all the shown distances to the mirror, while the higher-order modes do not reach the threshold at L < 2.7 cm. For the pump spot radius of 50 μm, the fundamental mode remains above the threshold. However, the next mode also lies above the threshold at L < 2.9 cm. The decrease in the mode decrement μ demonstrated in Fig. 5 with increasing the pump spot radius is explained by a better overlap of the mode field with the excitation region. The characteristic mode radius is determined first of all by the curvature radius of the external mirror and by the distance to it. The optimal situation for discrimination of higher-order modes corresponds to an approximate equality of dimensions of the pump beam and fundamental mode. This approximate equality occurs in the minimum of the curve for r_0 = 20 μm at L = 2.8 cm.

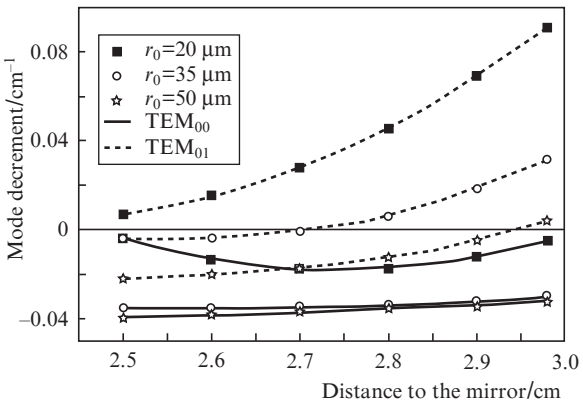

Figure 5. Dependences of the TEM_{00} and TEM_{01} mode decrements μ on L at an equivalent pump current of 400 mA and different pump spot radii.

More complex effects are observed in the region of L from 2 to 2.5 cm. Figure 6 presents the decrements of the fundamental mode, of the second radial mode, and of the first angular mode as functions of L for a pump spot radius of 25 μm and an equivalent current of 200 mA. The minima of each of the curves approximately correspond to the condition when the mode and pump spot sizes are close to each other. Both higher-order modes are below the excitation threshold at all distances. However, the fundamental mode decrement

demonstrates an unexpected behaviour. The fundamental mode lies below the threshold at the distances L = 2.2–2.35 cm. This is explained by the existence of a radially inhomogeneous phase incursion in 25 QWs of the heterostructure, which qualitatively corresponds to a defocusing lens. The appearance of a cuspidal point on the mode decrement plot relates to a jump to the fundamental mode with a different radial structure.

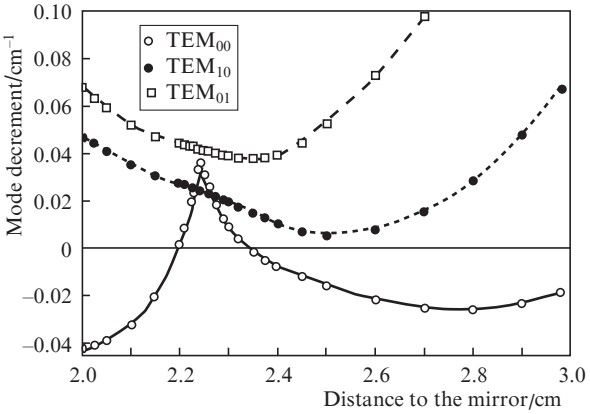

Figure 6. Dependences of the TEM_{00}, TEM_{10}, and TEM_{01} mode decrements μ on L at an equivalent injection current of 400 mA and a pump spot radius of 25 μm.

4.2. Calculation of lasing and fundamental mode stability

To estimate variations caused in the laser beam power and angular beam divergence by changes in L, we performed a series of calculations of lasing at the fundamental mode for different pump spot radii at an equivalent injection current of 400 mA (Fig. 7). As in the experiment, the calculated fundamental mode power only slightly depends on the cavity length at rather large radii of the excitation region. The general decrease in the power at $r_0 > 25$ μm is associated with decreasing excess of the pump density over the threshold. In experiment we observed lower laser powers, which, obviously, is caused by additional losses of laser radiation due to scattering by multiple interfaces of the studied heterostructure and by the surfaces of the sapphire substrate, which was not taken into account in the calculation. The divergence angle of the fundamental mode slowly increases with increasing L (Fig. 7b). This increase is mainly caused by a decrease in the mode diameter in the active heterostructure as the cavity configuration becomes closer to semiconcentric. The experimental divergence angle of 7.5 mrad measured at L = 2.5 cm agrees well with the calculated data.

The calculation results demonstrated in Fig. 7a for r_0 = 20 μm show a sharp increase in the power as L approaches 3.0 cm, which was not observed in experiment and is related to diffraction losses at the edge of the output mirror. Indeed, the mode size at the output mirror in this situation increases and, as illustrated in Fig. 8, becomes larger than the 400-μm diameter of the output mirror used in the calculation. In the experiment, we used a mirror of a larger diameter, and the losses caused by the propagation of radiation outside the mirror were absent. However, we observed a sharp (up to several degrees) increase in the output beam divergence, which agrees with the calculation results shown in Fig. 7b.

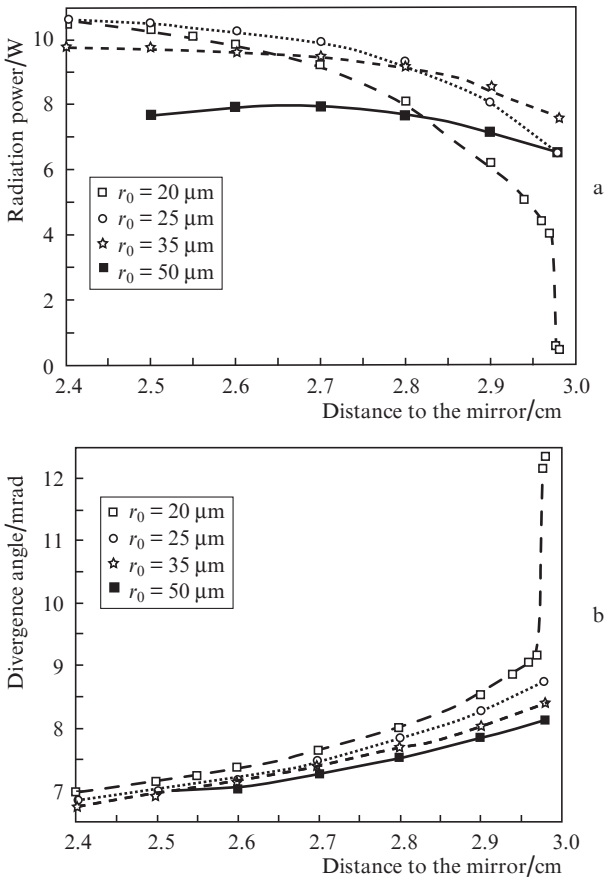

Figure 7. Dependences of the output power (a) and of the far-field divergence angle $\theta_{0.5}$ containing half of the output power (b) on L at an equivalent injection current of 400 mA and different pump spot radii.

The calculated dependence of the fundamental mode power on the equivalent injection current is shown in Fig. 9 for r_0 = 25 μm and L = 2.5 cm. By extrapolation to zero laser power, we found the threshold equivalent current to be $J_{th} \approx 50$ mA, which qualitatively agrees with the experimental value of 35 mA ($J^b_{th} \approx 0.2$ mA). Our calculations predict an improvement of the optical quality of the output beam with increasing power.

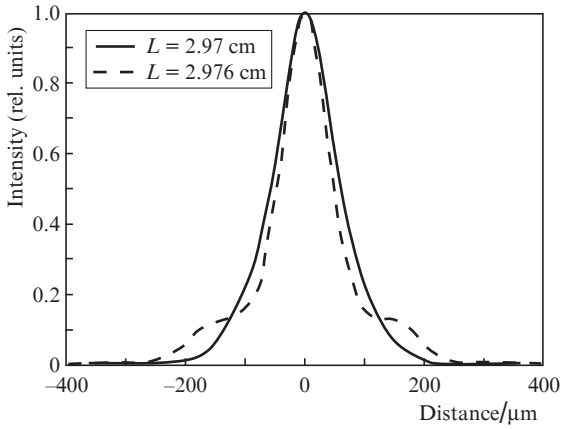

Figure 8. Transverse intensity distribution at the output mirror for a generated mode of a VCSEL with an external mirror at a pump spot radius of 20 μm, an equivalent injection current of 400 mA, and different L.

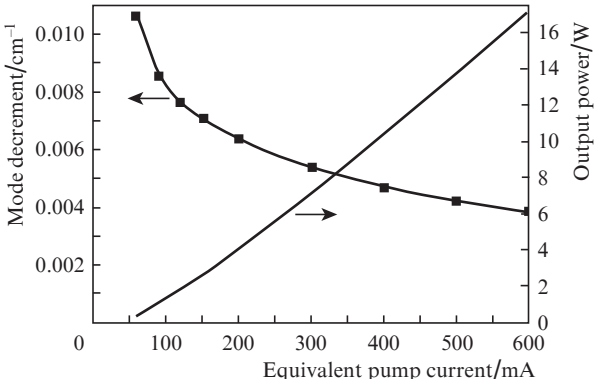

Figure 9. Laser power for the fundamental mode and TEM_{10} mode decrement μ as functions of the equivalent pump current in a VCSEL with an external mirror at $r_0 = 25$ μm and $L = 2.5$ cm.

The limiting current of single-mode lasing with respect to the excitation of higher modes was found by solving a linear problem in which the gain and refraction profiles in QWs are formed by the fundamental mode and are frozen [10]. The single-mode lasing stability is disturbed when the decrement for any of higher-order modes is $\mu \geqslant 0$. As is shown in Fig. 9, at pump currents corresponding to the fast-electron-beam peak currents used in the experiment, the competing (closest to the threshold) mode remains below the threshold. Thus, single-mode lasing at the given parameters remains stable, which agrees with experimental data. The use of an external mirror significantly extends the range of pump currents exciting single-mode lasing with respect to the same structure without an external mirror, for which the theory predicts that the critical current at which multimode lasing begins exceeds the lasing threshold only by a factor of 1.5 [7].

5. Conclusions

The developed numerical method of calculating a VCSEL with an external mirror allows one to find the spatial profiles and determine the power and optical beam quality of a generated mode. The characteristic time of calculation of one construction with a resonance grating of 25 QWs is about one hour when using a Pentium IV PC. The created program makes it possible to determine the lasing threshold for the fundamental mode and determine its characteristics as functions of the pump current and external cavity parameters. Our software package provides the possibility of finding the excitation threshold for higher-order modes against the background of the fundamental-mode-induced distributions of the gain and nonlinear part of the refractive index, which determines the maximum output power achievable in the single-mode regime. It is shown that, in agreement with experiment, at a distance to the external mirror of 2.5 cm and a pump spot radius of 25 μm, the higher-order modes remain below the excitation threshold in the entire studied region of pump currents.

Acknowledgements. This work was partly supported by the Russian Foundation for Basic Research (Grant Nos 08-02-00796-a and 10-02-00741).

References

1. Okhotnikov O.G. *Kvantovaya Elektron.*, **38** (12), 1083 (2008) [*Quantum Electron.*, **38** (12), 1083 (2008)].
2. Piprek J., Björlin S., Bowers J.E. *IEEE J. Quantum Electron.*, **37**, 127 (2001).
3. Bondarev V.Yu., Kozlovskii V.I., Krysa A.B., Popov Yu.M., Skasyrskii Ya.K. *Kvantovaya Elektron.*, **34** (10), 919 (2004) [*Quantum Electron.*, **34** (10), 919 (2004)].
4. Bondarev V.Yu., Kozlovsky V.I., Krysa A.B., Kuznetsov P.I., Sannikov D.A., Skasyrsky Ya.K., Tiberi M.D., Popov Yu.M. *Proc. SPIE Int. Soc. Opt. Eng.*, **6637**, 663707 (2007).
5. Bogatov A.P., Eliseev P.G. *Kvantovaya Elektron.*, **12** (3), 465 (1985) [*Quantum Electron.*, **15** (3), 308 (1985)].
6. Rao H., Steel M. J., Scarmozzino R., Osgood R.M., Jr. *IEEE J. Quantum Electron.*, **37**, 1435 (2001).
7. Vysotskii D.V., Elkin N.N., Napartovich A.P., Troshchieva V.N., Kozlovskii V.I., Lavrushin B.M. *Kvantovaya Elektron.*, **39** (11), 1028 (2009) [*Quantum Electron.*, **39** (11), 1028 (2009)].
8. Elkin N.N., Napartovich A.P., Troshchieva V N., Vysotsky D.V. *Lect. Notes Comput. Sci.*, **4310**, 542 (2007).
9. Fox A.G., Li T. *IEEE J. Quantum Electron.*, **QE-2**, 774 (1966).
10. Elkin N.N., Napartovich A.P., Troshchieva V.N., Vysotsky D.V. *Lect. Notes Comput. Sci.*, **5434**, 273 (2009).
11. Hadley G.R., Hohimer J.P., Owyoung A. *IEEE J. Quantum Electron.*, **23**, 765 (1987).
12. Siegman A. E. *Opt. Lett.*, **1**, 13 (1977).
13. Anan'ev Yu.A. *Opticheskie rezonatory i problemy raskhodimosti lazernogo izlucheniya* (Optical cavities and the problem of laser-radiation divergence) (Moscow: Nauka, 1979).
14. Vainshtein L.A. *Otkrytye rezonatory i otkrytye volnovody* (Open cavities and open waveguides) (Moscow: Sov. Radio, 1966).